Annals of Nuclear Medicine Vol. 11, No. 4, 307–313, 1997

Performance evaluation of a large axial field-of-view PET scanner: SET-2400W

Takehiko FUJIWARA,* Shoichi WATANUKI,* Seiichi YAMAMOTO,*** Masayasu MIYAKE,* Shinya SEO,* Masatoshi ITOH,* Keizou ISHII,* Hikonojyou ORIHARA,* Hiroshi FUKUDA,** Tomohiko SATOH,**** Keishi KITAMURA,**** Kazumi TANAKA**** and Shigekazu TAKAHASHI****

Cyclotron and Radioisotope Center, Tohoku University
**Department of Radiology and Nuclear Medicine, Institute of Development, Aging and Cancer, Tohoku University*
***Department of Electrical Engineering, Kobe City College of Technology*
****Shimadzu Corporation, Kyoto*

The SET-2400W is a newly designed whole-body PET scanner with a large axial field of view (20 cm). Its physical performance was investigated and evaluated. The scanner consists of four rings of 112 BGO detector units (22.8 mm in-plane × 50 mm axial × 30 mm depth). Each detector unit has a 6 (in-plane) × 8 (axial) matrix of BGO crystals coupled to two dual photomultiplier tubes. They are arranged in 32 rings giving 63 two-dimensional image planes. Sensitivity for a 20-cm cylindrical phantom was 6.1 kcps/kBq/m*l* (224 kcps/μCi/m*l*) in the 2D clinical mode, and to 48.6 kcps/kBq/m*l* (1.8 Mcps/μCi/m*l*) in the 3D mode after scatter correction. In-plane spatial resolution was 3.9 mm FWHM at the center of the field-of-view, and 4.4 mm FWHM tangentially, and 5.4 mm FWHM radially at 100 mm from the center. Average axial resolution was 4.5 mm FWHM at the center and 5.8 mm FWHM at a radial position 100 mm from the center. Average scatter fraction was 8% for the 2D mode and 40% for the 3D mode. The maximum count rate was 230 kcps in the 2D mode and 350 kcps in the 3D mode. Clinical images demonstrate the utility of an enlarged axial field-of-view scanner in brain study and whole-body PET imaging.

Key words: positron emission tomography, performance evaluation, whole body scan, 2D

INTRODUCTION

POSITRON EMISSION TOMOGRAPHY (PET) has become established as a technique to measure *in vivo* tissue function. The PET scanners developed from a single ring of detectors and evolved into multiple stacks of detector rings with a rapid growing demand for increased axial coverage. The axial field-of-view (FOV) of modern multi-ring PET scanners is around 150 mm and spatial resolution is around 4–6 mm FWHM in the 2D data acquisition.[1–4] They were designed to cover whole organs such as brain and heart for dynamic studies with nearly isotropic high spatial resolution. For whole-body scanning, the number of bed positions and total scanning time were reduced in comparison with 10 cm axial FOV scanners.[1] The larger axial FOV of PET scanner, therefore, seems to offer a great advantage in clinical studies.

The extended axial FOV and improved spatial resolution of PET scanners lead to a new acquisition technique, three dimensional (3D) acquisition and reconstruction.[5,6] The advantage of the 3D data acquisition is sixfold to eightfold higher sensitivity than the 2D data acquisition. The sensitivity of the 3D PET scanner is proportional to the square of the axial FOV if one can use full acquisition data for the 3D reconstruction,[7] but there is little gain of sensitivity at the edge of the axial FOV because accidental and scatter coincidences are increased in the 3D acquisition.[7–9] This means that the effective axial FOV is decreased in the 3D data acquisition compare with the 2D data acquisition of the same scanner. The larger axial FOV of PET scanner seems to be preferable to the 3D data acquisition.

Received April 14, 1997, revision accepted August 20, 1997.

For reprint contact: Takehiko Fujiwara, M.D., Ph.D., Division of Cyclotron Nuclear Medicine, Cyclotron and Radioisotope Center, Tohoku University, Aoba, Aramaki, Aoba-ku, Sendai 980–77, JAPAN.

E-mail: fujiwara@cyric.tohoku.ac.jp

The Shimadzu SET-2400W is a new whole-body PET scanner with an axial FOV of 20 cm. It works in both 2D and 3D modes. In this paper, its physical performance was investigated and evaluated in phantom studies. Some clinical images obtained with the scanner are also presented.

MATERIALS AND METHODS

System description

The scanner consists of four rings of 112 BGO detector units (22.8 mm in-plane × 50 mm axial × 30 mm depth). Each detector unit has a 6 (in-plane) × 8 (axial) matrix of BGO crystals coupled to two dual photomultiplier tubes (Hamamatsu R1548).[10] Crystal size is 3.8 mm (in-plane), 6.25 mm (axial) and 30 mm (depth). These are arranged in 32 rings with 672 crystals each giving 63 two-dimensional image planes. The axial FOV is 20 cm. The ring diameter is 850 mm and the patient port diameter is 590 mm. Signals from the photomultiplier tubes are processed to the position of the crystal in which gamma photon hits by using a coincidence time window of 15 ns. Position non-linearity and energy non-uniformity of the detector unit are corrected in realtime. In the 2D mode, axial coincidence path acceptance can be controlled from 1 to 8 to optimize sensitivity and axial resolution. The system has lead septa 1 mm thick and 95 mm long for the 2D mode. The septa can be automatically retracted for the 3D mode. Sixty-three sinograms are stored in a large scale of acquisition memory (1 GB) in the 2D mode. In the 3D mode, all possible coincidence pairs of 1,024 sinograms are stored in the same memory. Corrections for dead time and decay of radioisotope can be performed in real-time in the memory.[11,12] A ^{68}Ge-^{68}Ga external line source with 370 MBq (10 mCi) can be orbited in a 640 mm radius to measure blank scan and transmission scan data. The system design parameters of the SET-2400W are listed in Table 1.

Table 1 System parameters of SET-2400W

Block detector design	6 (in-plane) × 8 (axial)
Number of rings	32 rings
Number of slices	63 slices
Number of detector blocks	448
Crystal size (mm^3)	3.8 × 6.25 × 30
Number of crystals	21,504
Image plane spacing (mm)	3.125
Detector ring diameter (mm)	850
Patient aperture (mm)	595
Field of view (mm)	
Axial	200
Transverse	590
For whole body scan	1,750

Sensitivity

The sensitivity of the PET was measured with a 20-cm inner diameter by 25-cm long cylindrical acrylic phantom filled with ^{18}F solution of approximately 3.7 kBq/ml (0.1 μCi/ml). The activity in the phantom was determined by measuring the total amount of radioactivity injected into the phantom by a calibrated well counter. The lower energy threshold was set at 292 keV. The total count rate of the PET scanner was measured for the phantom and the true sensitivity was calculated. Measurements were done for various axial coincidence path acceptances in the 2D mode with septa extended. Measurements were also done in the 3D mode with septa retracted.

Spatial resolution

In-plane spatial resolution was measured with a ^{18}F line source filling a stainless steel tube with an inner diameter of 0.5 mm. The source was held in air parallel to the longitudinal axis of the scanner at five positions: 0, 5, 10, 15 and 20 cm from the center of the FOV. At least 5×10^5 true counts per plane were acquired and images were reconstructed in a 256 × 256 matrix with a pixel size of 0.5 mm using a ramp filter with a cutoff frequency of 0.5 cycle/mm. Profiles of the images were analyzed in radial and tangential FWHM. The axial resolution was measured with a ^{22}Na point source with a diameter of 2 mm. The source was moved stepwise in 0.5 mm increments through the axial FOV, and true plus scatter counts of each slice were plotted. Each measurement was recorded at five different positions (r = 0, 5, 10, 15 and 20 cm) from the center of the FOV. The FWHMs in each slice were estimated by linear interpolation. Measurements were done only in the 2D mode for a fixed axial coincidence path acceptance (5 for direct planes and 6 for cross planes).

Scatter fraction

A scatter fraction was measured by using a ^{18}F line source contained in a tube of 0.5 mm inner diameter placed in three different positions (0, 4, and 8 cm from the center) in a 20-cm cylindrical phantom filled with water. Since the axial FOV of SET-2400W was longer than the length of the standard phantom (18.5 cm), data for the phantom placed at several positions of the axial FOV were acquired in the both septa extended and the septa retracted mode. The lower energy threshold was set at 292 keV. The scatter fraction was estimated from the projection by using the equation published in the NEMA standard.[5] The scatter fraction for individual slice was estimated. All measurements in the 2D mode were performed for a fixed axial coincidence path acceptance (5 for direct planes and 6 for cross planes).

Count rate

The count rate performance was measured with a 20-cm inner diameter by 25-cm long cylindrical phantom filled with ^{11}C water solution. After the solution of 2,220 MBq (60 mCi) was injected into the phantom, the total count

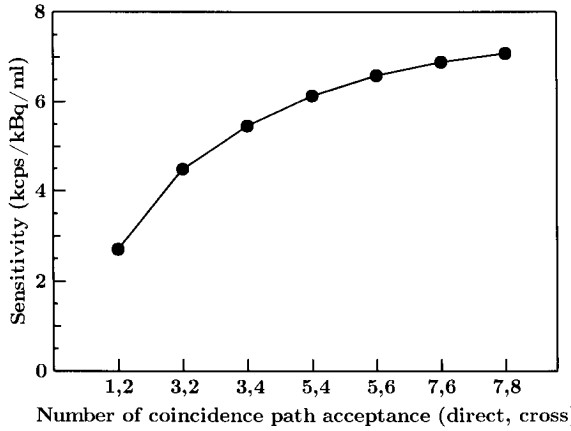

Fig. 1 The relation between total true sensitivity and number of coincidence path acceptances. In the clinical study, five for direct planes and six for cross planes are used. The sensitivity per slice is 96.8 cps/kBq/m*l* (3.6 kcps/μCi/m*l*) in this mode.

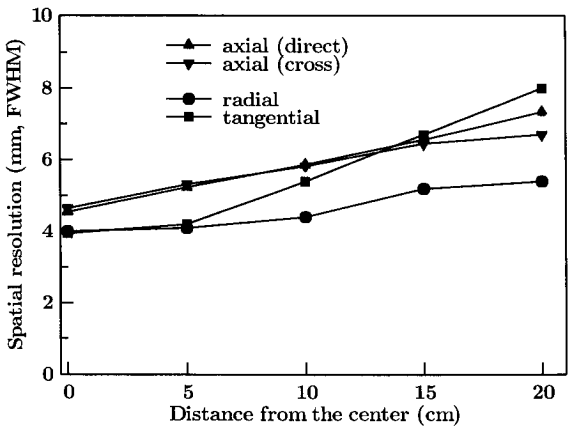

Fig. 2 Spatial resolution of the SET-2400W as a function of the distance from center. The spatial resolution at the center is less than 4.5 mm in all directions for typical patient studies.

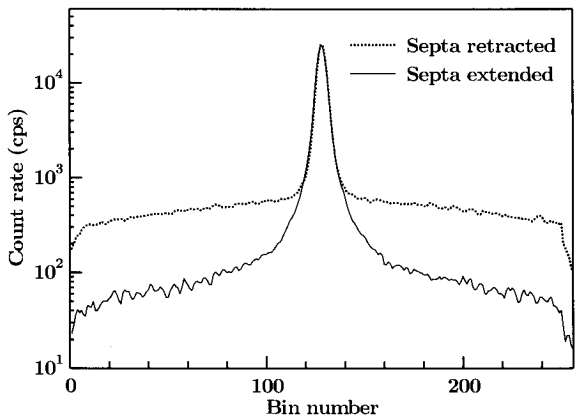

Fig. 3 Average sinograms from a line source centered in a water-filled phantom, with and without septa.

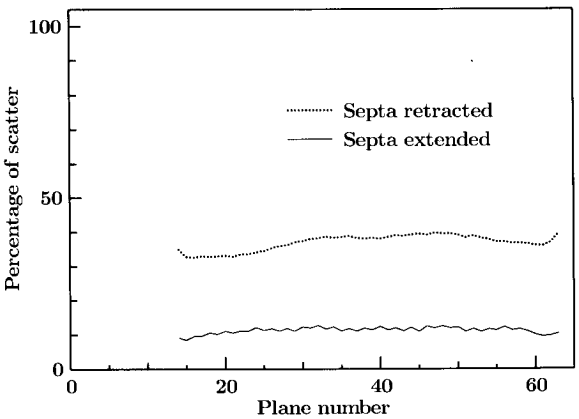

Fig. 4 The variation of the scatter fraction with one of axial positions as a function of the axial position with and without septa.

rate was measured. The random coincidence rate was simultaneously measured with the delayed coincidence window. The data were taken at 3-min intervals until the count rate losses of the true coincidence rates and the random rates became negligible. The individual acquisition duration was 2.5 min. In the 2D mode, measurement was done only for a fixed axial coincidence path acceptance (5 for direct planes and 6 for cross planes). A similar experiment but with a factor of 6 lower activity was done with the 3D mode.

RESULTS

Sensitivity

Total true sensitivity in the 2D with septa extended was changed from 2.70 kcps/kBq/m*l* (100 kcps/μCi/m*l*) to 7.08 kcps/kBq/m*l* (262 kcps/μCi/m*l*) according to the number of coincidence path acceptance. The relation between sensitivity and number of coincidence path acceptances is shown in Figure 1. Sensitivity in the 2D clinical mode (numbers of coincidence path acceptances: 5 for direct planes and 6 for cross planes) was 6.1 kcps/kBq/m*l* (224 kcps/μCi/m*l*) after scatter subtraction. Total sensitivity in the 3D mode was 48.6 kcps/kBq/m*l* (1.8 Mcps/μCi/m*l*) after subtraction of scatter component.

Spatial resolution

Figure 2 shows the relation between in-plane spatial resolution and the distance from the center of the FOV. In-plane resolution was 3.9 mm FWHM at the center of FOV, 4.4 mm FWHM tangentially and 5.4 mm FWHM radially at 100 mm from the center. Figure 2 also shows the relation between axial resolution and the distance from the center. Average axial resolution for direct slices was 4.5 mm FWHM at the center and 5.9 mm FWHM at 100 mm from the center. For cross slices, axial resolution increased from 4.6 mm FWHM at the center to 5.8 mm FWHM at a radius of 10 cm. The change in transaxial resolution is 18–38% from the center to 10 cm out and the axial resolution changes by 26–31%.

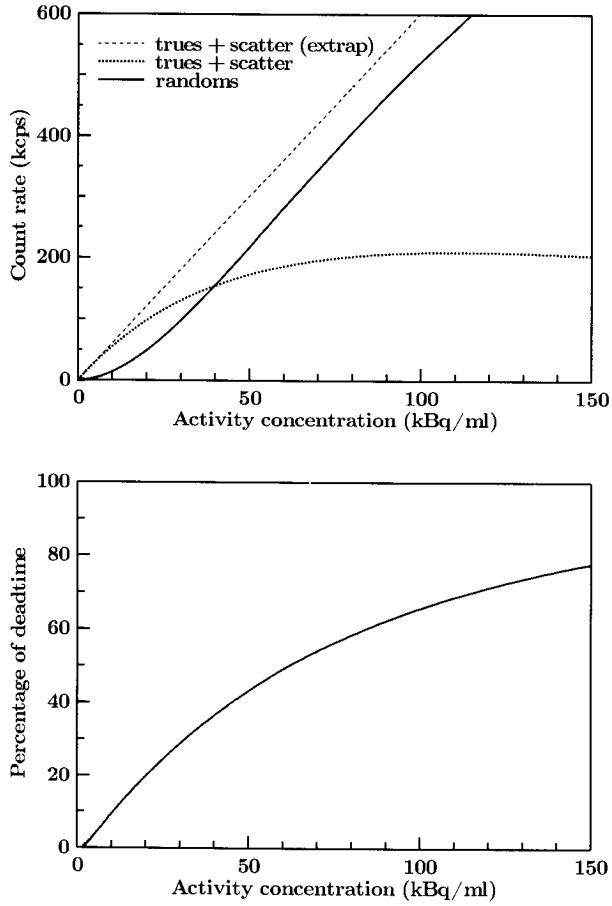

Fig. 5 High count rate characteristics using a performance phantom filled with ^{18}F in water with septa extended mode. In the upper figure, the true and random count rates are plotted as a function of activity concentration. In the lower figure, the percent deadtime is calculated from the ratio of trues + scatter-to-extrapolated trues + scatter.

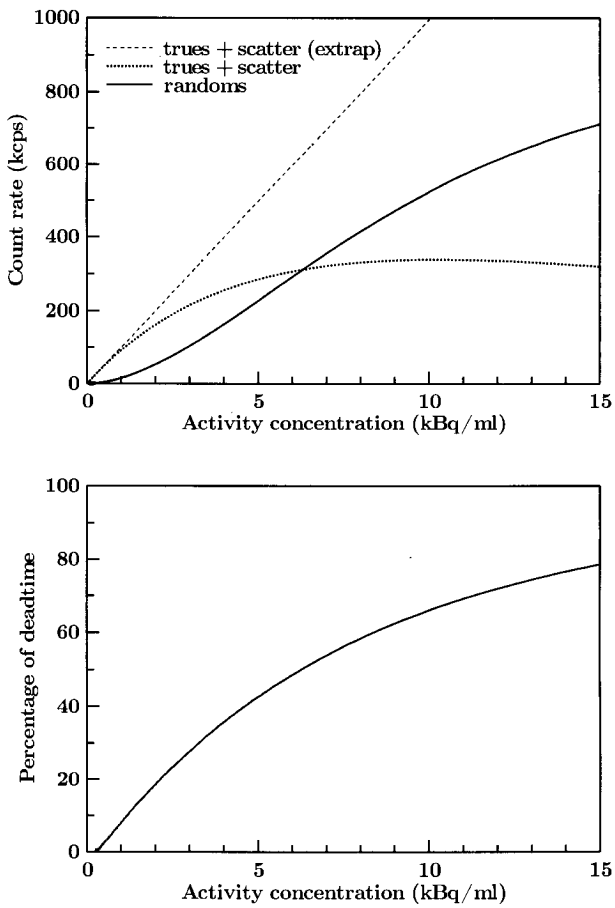

Fig. 6 Same as in Figure 5, but with the 3D (septa retracted) mode.

Scatter fraction

The spatial distribution of scatter components for a line source is shown in Figure 3. The average scatter fraction among all slices for septa in was 8%. For septa out, the average scatter fraction was increased to 40%. The variation in the scatter fraction with one of the axial positions is shown in Figure 4. Slight increases toward the center of the axial FOV for the septa extended mode and septa retracted mode are seen.

Count rate performance

Total count rate performances for the 2D mode and the 3D mode are shown in Figures 5 and 6. The maximum count rate for all slices was 230 kcps in the 2D mode and 350 kcps in the 3D mode. The noise equivalent count rate (NECR) is shown in Figure 7 as a function of the radioactivity concentration. The NECR was calculated from the true (T), scatter (S) and random (R) rates.

$$NECR = T/(1 + S/T + 2R/T)$$

The maximum NECRs of 73.6 kcps and 95.8 kcps are reached at radioactivities of 43.7 kBq/m*l* (1.18 μCi/m*l*) for the 2D mode and 4.44 kBq/m*l* (0.12 μCi/m*l*) for the 3D mode, respectively. Comparison of NECR curves shows this index to be higher for the 3D mode than for the 2D mode at radioactivity concentrations under 15.5 kBq/m*l* (0.42 μCi/m*l*). The maximum NECR for the 3D mode is 30% higher than that for the 2D mode.

Imaging studies

The imaging performance of the SET-2400W was tested for several applications. A resolution phantom filled with ^{18}F activity was scanned in the 2D mode. The data were reconstructed using a Butterworth-ramp filter with a cut-off frequency of 0.5 cycle/pixel. The image of the resolution phantom is shown in Figure 8. Clear separation of the 2.5 mm hot spot is seen.

The whole brain of a normal volunteer given 370 MBq (10 mCi) of ^{18}F-FDG was scanned over a 60 min acquisition period starting at 30 min after injection in the 2D mode. The 63 transverse images were resliced to sagittal and coronal images for the 3D display (Fig. 9).

With the dopamine D_2 receptor ligand ^{11}C-YM-09157-1 (^{11}C-YM), the accumulations of the tracer in the striatum

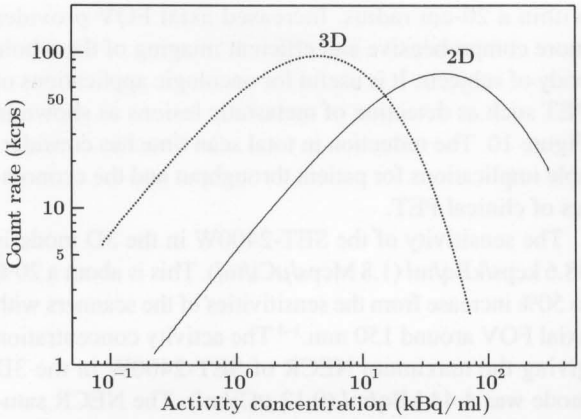

Fig. 7 Comparison of noise equivalent count rate curves for the 2D (septa extended) mode and the 3D (septa retracted) mode.

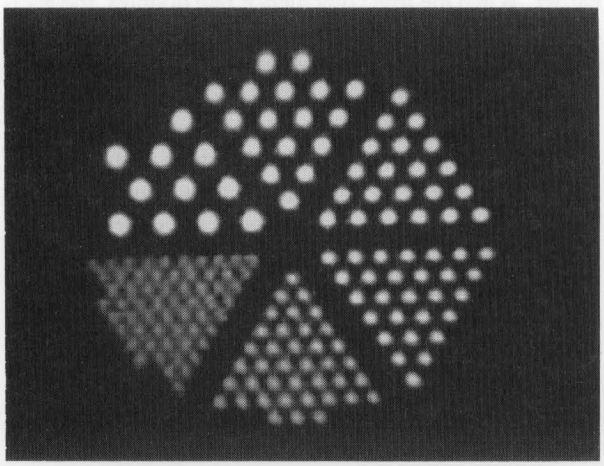

Fig. 8 Image obtained with the resolution phantom. The diameters of dots are equal in each segment, ranging from 2 mm to 5 mm with 0.5 mm increment. The center-to-center dot spacing is four times the diameter. The sinogram contains 6.5×10^7 counts.

were compared with the 2D scan and the 3D scan (Fig. 10). Imaging of the 2D began at 90 min after injection of 185 MBq (5 mCi) of ^{11}C-YM and the 3D emission scan started after the 2D scan. The accumulations of the ^{11}C-YM in the striatum were clearly visualized in the 3D images.

The whole-body of the operated cervical uterine cancer patient was scanned 30 min after intravenous injection of 370 MBq (10 mCi) of ^{18}F-FDG in the 2D mode. The data from five contiguous axial FOVs were reformatted into coronal projections (Fig. 11). This display allows rapid localization of multiple bone metastases. For this particular case, the total emission scan time was 25 min. A 5-min post-injection transmission scan for each position was performed after emission scans.

A whole-body of a normal subject was scanned in the 3D mode with the increment of table position at 1-min scan period after injection of 99.9 MBq (2.7 mCi) of ^{18}F-

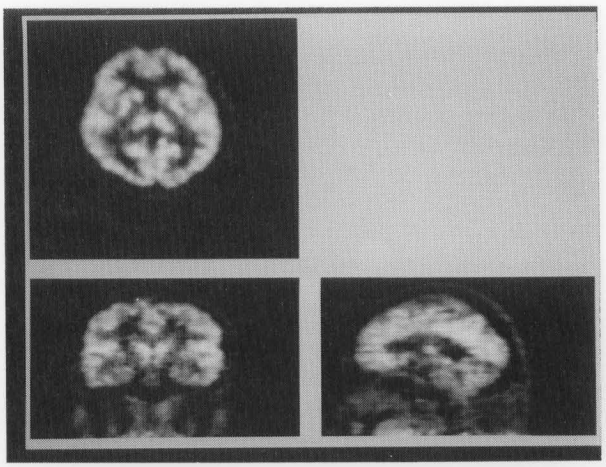

Fig. 9 Brain images of the accumulation of ^{18}F-FDG in a normal volunteer. A total of 6.4×10^6 counts per center slice was obtained. All 63 images were resliced to coronal, and sagittal images. The advantage of a large axial FOV is that patient positioning is not as critical in terms of imaging the entire brain.

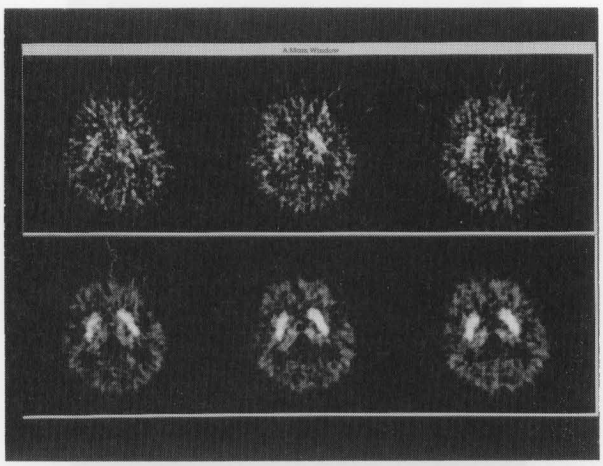

Fig. 10 Comparison of ^{11}C-YM-09151-2 studies of the same subject on a 10-min 2D scan (top) and a 10-min 3D scan (bottom). The corresponding sinograms contain 4.7×10^5 counts (2D) and 5.0×10^6 counts (3D).

FDG. The 2D transmission data in the 5 min frames were obtained and the 3D attenuation correction factors were computed from the forward projection of the 2D attenuation maps. Only 9 min emission scan time was necessary to obtain an overview of the FDG uptake in all the organs of interest including brain, heart, and bladder (Fig. 12). To reduce the scattered photons in the final images, the 3D reconstructed images are digitally post processed with a low pass filter and these images are weighted and subtracted from the original 3D images to remove the scattered photons.[13]

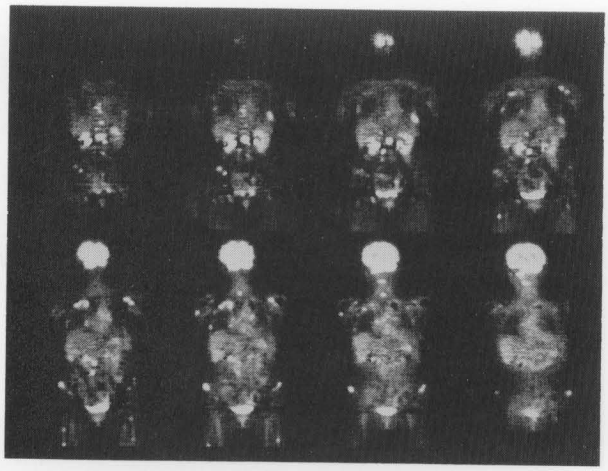

Fig. 11 Coronal sections of 2D ^{18}FDG whole-body scan of cervical uterine cancer patient depict multiple bone metastases.

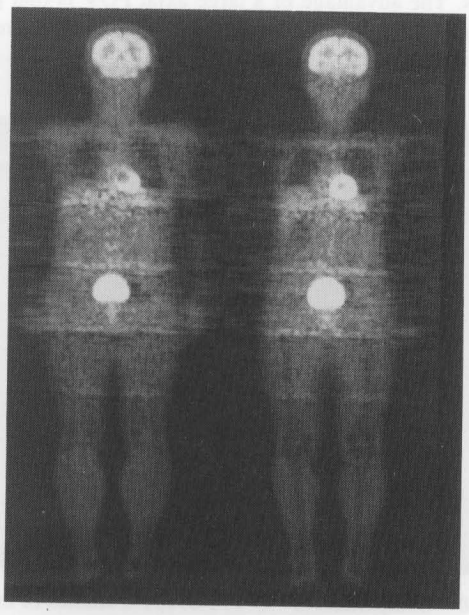

Fig. 12 Whole-body 3D PET images at rest show normal distribution of ^{18}FDG in coronal sections 90 min after injection. The emission scan time for each axial position was 1 min. Since 3D acquisition data from edge of the field-of-view were used in this study, some reconstruction artifacts are seen.

DISCUSSION

The SET-2400W has a large 20 cm axial field of view. This enables brain studies covering the entire brain or heart with no need to shift the subject's position or to center the organ precisely. The results show nearly cubic spatial resolution better than 6 mm within a 10-cm radius and allow reslicing of the brain images for reorientation process. The resolution decreases further at greater distances from the center. This may lead to some distortion of images in body studies. However, the spatial resolution in all three directions never exceeds 8.0 mm FWHM within a 20-cm radius. Increased axial FOV provides more comprehensive and efficient imaging of the whole body of subjects. It is useful for oncologic applications of PET such as detection of metastatic lesions as shown in Figure 10. The reduction in total scan time has considerable implications for patient throughput and the economics of clinical PET.

The sensitivity of the SET-2400W in the 3D mode is 48.6 kcps/kBq/m*l* (1.8 Mcps/μCi/m*l*). This is about a 20% to 50% increase from the sensitivities of the scanners with axial FOV around 150 mm.[1–3] The activity concentration giving the maximum NECR of SET-2400W in the 3D mode was 4.44 kBq/m*l* (0.12 μCi/m*l*). The NECR saturated at lower activity than the scanners with axial FOV around 150 mm. This may be because the coincidence rates, especially accidental coincidence rates increase earlier. When the true coincidence rate doubles, the accidental coincidence rate increases to four times. The accidental coincidence may be one reason for saturation at lower activity.

The sensitivity in the 3D mode is eight times as high as that in the 2D mode. The main advantage of the 3D data acquisition is the detection of lower tracer concentrations. This is especially true in studies of the distribution of ligands for neuroreceptors. As shown in Figure 11, ^{11}C-YM-09151-2 images from the 3D acquisition showed better visualization of striatum than the 2D images with the same scanning time. Similar results can be expected for other neuroreceptor ligands. Another advantage of 3D data acquisition is the reduction in scanning time. It is useful not only for the study of patients for whom a long scan period is not possible because of their critical condition but also for whole body scanning. We found that even a 1-min ^{18}F-FDG emission scan for each position (9 min for the whole body) was enough to visualize the distribution of the radioisotope in the body. However, the transmission data in 4–8 min frames were inevitable before/after emission scans for attenuation correction with the present system configuration. To reduce total study time, new methods of attenuation correction such as single photon transmission and segmentation of attenuation images are necessary.[14,15]

The large increase in the scatter fraction of the measured coincidence events is a major problem in quantitative 3D data acquisition. Since the scatter fraction of the scanner in the 3D mode was 40%, the scattered radiation must be removed from the final images to compare the quantitative performance of 2D imaging and 3D imaging. Recently, several 3D scatter correction techniques have been proposed such as the dual-energy window approach and the convolution-subtraction method.[16,17] At Tohoku University, research on scatter correction is under way. Thus scatter subtraction in the 3D mode of this study is preliminary and further evaluation is necessary.

CONCLUSION

The performance data sets of a newly designed whole-body PET (SET-2400W) are presented. Clinical images demonstrate the utility of enlarged axial FOV PET in brain study and whole-body imaging although the scanner has some limitations.

REFERENCES

1. Wienhard K, Eriksson L, Grootoonk S, Casey M, Pietrzyk U, Heiss W-D. Performance evaluation of the positron scanner ECAT EXACT. *J Comput Assist Tomogr* 16: 804–813, 1992.
2. Wienhard K, Dahlbom M, Eriksson L, Michel C, Bruckbauer T, Pietrzyk U, et al. The ECAT EXACT HR: Performance of a new high resolution positron scanner. *J Comput Assist Tomogr* 18: 110–118, 1994.
3. DeGrado TR, Turkington TG, Williams JJ, Stearns CW, Hoffman JM, Coleman RE. Performance characteristics of a whole-body PET scanner. *J Nucl Med* 35: 1398–1406, 1994.
4. Iida H, Miura S, Kanno I, Ogawa T, Uemura K. A new PET camera for noninvasive quantitation of physiological functional parametric images. Headtome-V-Dual. *In* Quantification of Brain Function Using PET. Myers R et al. (eds.), California, Academic Press, pp. 57–61, 1996.
5. Karp JS, Daube-Witherspoon ME, Hoffman EJ, Lewellen TK, Links JM, Wong W-H, et al. Performance standards in positron emission tomography. *J Nucl Med* 32: 2342–2350, 1991.
6. Colsher JG. Fully three-dimensional positron emission tomography. *Phys Med Biol* 25: 103–115, 1980
7. Defrise M, Townsend DW, Geissbuhler A. Implementation of three-dimensional image reconstruction for multi-ring tomographs. *Phys Med Biol* 35: 1361–1372, 1990.
8. Cherry SR, Dahlbom M, Hoffman EJ. 3D PET using a conventional multislice tomograph without septa. *J Comp Assist Tomogr* 15: 655–668, 1991.
9. Townsend DW, Geissbuhler A, Defrise M, Hoffman EJ, Spinks TR, Bailey DL, et al. Fully three-dimensional reconstruction for a PET camera with retractable septa. *IEEE Trans Med Imag* MI-10: 505–512, 1991.
10. Yamamoto S, Iida H, Miura S, Kanno I. Development of a 2-dimensional gamma ray position sensitive detector for PET. *Radioisotopes* 45: 229–235, 1996. *(in Japanese)*
11. Yamamoto S, Amano M, Miura S, Iida H, Kanno I. Deadtime correction method using random coincidence for PET. *J Nucl Med* 27: 1925–1928, 1986.
12. Iida H, Miura S, Kanno I, Murakami M, Takahashi K, Uemura K, et al. Design and evaluation of HEADTOME IV: a whole body positron emission tomograph. *IEEE Trans Nucl Sci* NS-36: 1006–1010, 1989.
13. Sashin D, Mintun MA. Development of scatter correction techniques for quantitative 3D imaging in a whole body PET scanner with the septa retracted. *IEEE Conf Nucl Sci and Med Imag*; 1332–1334, 1994.
14. Karp JS, Muehllehner G, Qu H, Yan XH. Singles transmission in volume-imaging PET with a ^{137}Cs source. *Phys Med Biol* 40: 929–944, 1995.
15. Meikle SR, Dahlbom M, Cherry SR. Attenuation correction using count-limited transmission data in positron emission tomography. *J Nucl Med* 34: 143–150, 1993.
16. Grootoonk S, Spinks TJ, Sashin D, Spyrou NM, Jones T. Correction for scatter in 3D brain PET using a dual energy window method. *Phys Med Biol* 41: 2757–2774, 1996.
17. Bailey DL, Meikle SR. A convolution-subtraction scatter correction method for 3D PET. *Phys Med Biol* 39: 412–424, 1994.